RESEARCH ARTICLE

Numerical Evaluation of Rudder Performance Behind a Propeller in Bollard Pull Condition

Diego Villa[1] · Michele Viviani[1] · Giorgio Tani[1] · Stefano Gaggero[1] · Dario Bruzzone[1] · Carlo Bonvino Podenzana[1]

Abstract

Correct evaluation of rudder performance is a key issue in assessing ship maneuverability. This paper presents a simplified approach based on a viscous flow solver to address propeller and rudder interactions. Viscous flow solvers have been applied to this type of problems, but the large computational requests limit (or even prevent) their application at a preliminary ship design stage. Based on this idea, a simplified approach to include the propeller effect in front of the rudder is considered to speed up the solution. Based on the concept of body forces, this approach enables sufficiently fast computation for a preliminary ship design stage, thereby maintaining its reliability. To define the limitations of the proposed procedure, an extensive analysis of the simplified method is performed and the results are compared with experimental data presented in the literature. Initially, the reported results show the capability of the body-force approach to represent the inflow field to the rudder without the full description of the propeller, also with regard to the complex bollard pull condition. Consequently, the rudder forces are satisfactorily predicted at least with regard to the lift force. However, the drag force evaluation is more problematic and causes higher discrepancies. Nevertheless, these discrepancies may be accepted due to their lower influence on the overall ship maneuverability performance.

Keywords Rudder–propeller interaction · RANS · Body forces · Actuator disk · Bollard pull

1 Introduction

Predicting rudder performance is a standard task in naval architecture (see, for example, Molland and Turnock 2007; Liu and Hekkenberg 2016; Han 2008; Simonsen 2000; Carlton et al. 2009). As the main maneuvering device of a ship, the rudder should be able to provide adequate maneuvering capability. At the preliminary design stage, the ship designer should be able to correctly predict the performance of the rudder. In general, a rudder is a simple lifting surface and extensive experimental data are available on its open-water performance (Molland and Turnock 1992; Fujii and Tuda 1961; Felli et al. 2009). On the contrary, once considered in the ship layout, the inflow field can be strongly inhomogeneous due to the presence of the hull wake, which becomes asymmetrical during maneuvers, and due to the effect of the propeller slipstream (Dubbioso et al. 2015; Crane et al. 1989; Lee et al. 2003; Krasilnikov et al. 2003). The hull wake in rectilinear motion results mainly in velocity reduction, which is commonly explored at the design stage by means of dedicated experimental tests and/or numerical predictions. The reliability of the numerical wake predictions has been demonstrated in the literature (see Wackers et al. 2015; Gaggero et al. 2014a; Kim et al. 2001; Stern et al. 1994; Gaggero et al. 2015). During a maneuver, the rudder can experience a highly complex flow field. The presence of the propeller in front of the rudder increases the inflow field complexity (rotational mean flow, rudder-tip vortex interaction, and others) both in the simple case of straight motion and, with increased complexity, during a maneuver (Simonsen and Stern 2003; Hochbaum 1998; Norrbin 1971). Ad hoc experimental tests to measure the flow field in maneuvering conditions may be onerous, at least at the preliminary design stage, and the reliability of numerical predictions remain arguable despite certain improvements (Durante et al. 2012; Stern et al. 2011; Di Mascio et al. 2015; Badoe et al. 2015).

Over the years, many semi-empirical approaches have been proposed (see Abkowitz 1980; Bertram 2002;

✉ Diego Villa
    diego.villa@unige.it

[1] Department of Electrical, Electronics and Telecommunication Engineering and Naval Architecture – DITEN, University of Genova, 16145 Genoa, Italy

Coraddu et al. 2013, which included asymmetrical conditions) to partially consider the propeller/hull interaction. These approaches proved to be sufficiently reliable in correspondence or in proximity to design conditions (i.e., with the propeller at design revolutions for cruise speed). However, when off-design conditions are considered (such as for the bollard pull condition), these formulations may be ineffective or may provide inaccurate data. Indeed, when a ship is at rest, the full force generated by the rudder is only determined by the accelerated flow of the propeller. Thus, the correct capturing of propeller and rudder interactions is even more crucial than in the design propeller functioning at cruise speed. As the bollard pull condition may be of interest for particular applications, such as maneuverability in harbor or dynamic positioning conditions for ships without azimuthal thrusters, developing numerical tools to ensure accurate prediction of rudder forces is necessary. These tools should be not too computationally demanding so that they can be used at preliminary design stages. The classical potential flow-based methods (as the lifting line/surface or panel methods) can be considered a good compromise between accuracy and computational cost; this characteristic has led to their widespread application in evaluating propeller performance. However, different from the propeller case, the rudder usually operates at large values of the angle of attack, which may lead to separated flow and even stalling in certain cases. This condition significantly reduces the reliability of potential codes (Carlton 2012; Katz and Plotkin 2001; Sheng et al. 2007), which should be applied carefully. However, adopting general viscous solvers can overcome such problems because, in the same framework, these solvers can include all the nonlinear effects such as flow separation or turbulent effects. Recently, various works have focused on this problem by considering a wide range of angles of attack (Badoe et al. 2015; Broglia et al. 2013). The results of these calculations may be used to properly tune simplified methods extensively adopted in the literature (Dubbioso and Viviani 2012) to account for the complex flow characteristics.

In the present study, a commercial viscous code based on the solution of Navier–Stokes equations is adopted. However, its application to the complete solution (rudder and propeller) could be extremely onerous at preliminary design stages. Thus, a hybrid method is proposed to make the application feasible by reducing the requested computational efforts. In particular, the propeller effect on the rudder is simulated via a body-force approach, which is able to drastically reduce the total computational effort. The study allows defining certain guidelines for rudder flow prediction, including the presence of the propeller and its influence on the rudder forces (without including hull interaction at the moment). Particular attention is devoted to the bollard pull condition, which traditional approaches generally fail to address.

2 Numerical Background

The numerical code adopted in the present work is the commercial viscous RANS solver Star-CCM+ v9 (CD-Adapco user manual n.d.). This code is capable of solving the flow field by adopting a general polyhedral mesh with a finite volume approach. The classical Navier–Stokes equations, which are presented in time-varying form for an incompressible flow, are used on the basis of the Reynolds hypothesis expressed in Eq. (1).

$$
\begin{cases}
\nabla \cdot U = 0 \\
\rho \dfrac{\partial \boldsymbol{U}}{\partial t} + \rho(U \cdot \nabla U) = -\nabla p + \mu \nabla^2 U + \nabla \cdot T_{\mathrm{Re}} + S_M
\end{cases}
\tag{1}
$$

where ρ and μ are respectively density and dynamic viscosity, which are incompressible flow characteristics; U is the mean velocity field; and p is the mean pressure field. The T_{Re} is the turbulent add-in term, which represents the contribution of the turbulence on the mean flow field. The last right-side term is the momentum source used to consider the volume force (e.g., gravity). This term may be evaluated explicitly or implicitly, depending on whether its value is proportional to the velocity field. In the present paper, this term is used to include the propeller force in the flow domain. This technique, already successfully adopted in other works (Berger et al. 2011; Villa et al. 2011; Rijpkema et al. 2013; Gaggero et al. 2017), may be used to generate the flow acceleration due to the propeller without needing a detailed solution for the flow field around the propeller blades (i.e., without including the rotating propeller into simulations). As the local blade force is independent from the local velocity (the total thrust is considered as a known value), the S_M term is computed explicitly.

In the present study, two approaches to include the propeller effect on the flow field are analyzed: the radially varying actuator disk and the full RANS approach. In the latter (indicated as "full RANS" in the following), the entire propeller geometry is discretized into a separate cylindrical region inside the domain, where a rotating mesh motion is imposed. A sliding interface technique is used to couple the rotating mesh and the fixed one. In the first procedure (indicated as "body force" in the following), the propeller effect is represented by means of radially distributed body forces; in this case, a proper source field (with strength distribution obtained from calculations on the propeller) is added to the momentum equations. Strength of axial and tangential momentum sources are set up to satisfy propeller thrust and torque.

Regarding the solver type, two approaches are explored in the present paper: steady approach and a transient one. The first uses a pseudo-time marching approach. This particular technique is based on the assumption that the solution of a set of steady PDEs can be considered as the solution of the correspondent time-varying PDE at an infinite time, exploiting the computational advantage of the inclusion of an optimal pseudo-time step (evaluated in accordance with the convective

Courant number). The second approach adopts the classical first-order implicit Euler approach. Both the steady and unsteady computations use the same algorithms to discretize and solve the PDE system. A segregation approach, together with the AMG linear solver, is used to invert the system of equations, and the SIMPLE algorithm is used to link pressure and velocity fields. The turbulence problem is closed with the *Realizable k-ε* model that, combined with a *two-layer wall* treatment, guarantees a good shear stress solution for the high Reynolds number with a $y+$ value, which is kept below 300. As a preliminary analysis, various standard two-equation turbulent models have been tested but no considerable variations in rudder forces have been found; consequently, the widely adopted *Realizable k-ε* model was selected as a good compromise between accuracy and computational effort.

As previously highlighted, having a fast and accurate flow solver is important that numerical techniques can be applied at the preliminary ship design stage. In a previous study (Bruzzone et al. 2014), various propeller approaches were used, ranging from a simple translational actuator disk to a fully viscous solution of the blade geometry. The results of that analysis showed the importance of the radial distribution of the propeller force (instead of a constant load distribution) in correctly evaluating the rudder force. The study concluded that the radially distributed actuator disk can be considered as the best compromise to save computational time without excessive simplifications, in particular if the inclusion of force unsteadiness due to propeller rotation is not of primary importance for the study (as in the present case). Consequently, the radially varying actuator disk model is selected for this study as an extension of the previous analyses conducted by Bruzzone et al. (2014), in which design conditions, with the propeller working at a moderate loading, were considered. In the present study, attention focuses on the more problematic bollard pull conditions.

3 Test Cases Analyzed

To validate the proposed approach, experimental measurements available in the literature are considered. In particular, a rudder investigated in the experiments by Molland and Turnock (1993a) is selected as a test case. The setup adopted in the experimental campaign is reported in Fig. 1. The tested rudder (named "number 2" in the original publication) is characterized by a NACA 4-digit cross section and a constant chord length along the span. It has an aspect ratio of 1.5 and a span of 1 m. This rudder has been tested in many different flow conditions and configurations in a wind tunnel to investigate the rudder/propeller interaction. In the present study, only the free-flow (rudder alone) and the bollard pull (rudder and propeller) cases are considered. The experimental tests were conducted with a modified version of the Wageningen B-series propeller in front of the rudder, with a diameter of
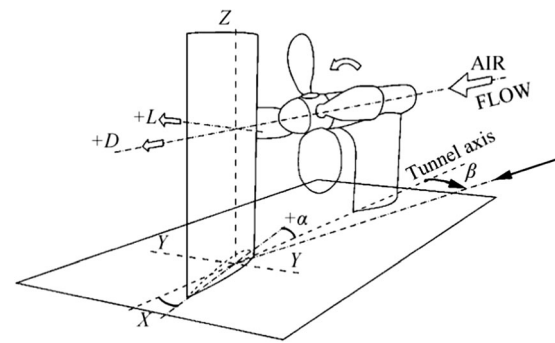

Fig. 1 Experimental setup (extracted by Molland and Turnock 1993a)

0.8 m. Two air-flow speeds are examined: 10 and 20 m/s (corresponding respectively to Reynolds number R_E equal to 4.4×10^5 and 8.8×10^5, considering only the free stream velocity without propeller effect).

In all the considered cases, the rudder deflection angle and angle of attack to the flow are equal (being flow only axial). In the following, this angle is indicated as α.

4 Mesh and Domain Setup

The mesh setup adopted for the computations is briefly described in this section. This setup was obtained after some preliminary tests (not reported for the sake of conciseness) and is reported in Fig. 2.

The domain is characterized by an inlet condition in front of the rudder/propeller and an outlet condition on all other boundaries to effectively consider the outflow generated by the rudder deflection. In the tests, to consider the mirror effect generated by the presence of the hull stern near the rudder, a plate was adopted, as shown in Fig. 1. To represent it, a wall boundary was set on one side of the rudder (yellow surface at the bottom of Fig. 2). With the rudder span as reference length, the domain had a width, length, and height equal to 3, 6, and 2.5 span lengths.
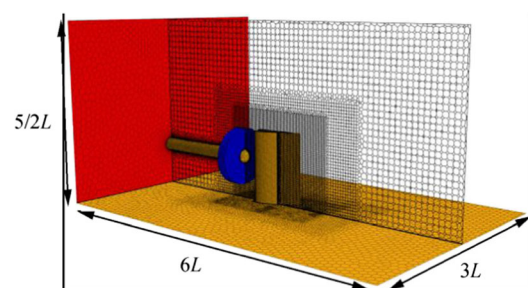

Fig. 2 Domain arrangement used in simulations: wall boundary in orange, inflow boundary in red, and propeller region in blue

Numerically, four types of boundary conditions were adopted in the simulations. For the wall boundaries, the classical no-slip condition was considered with a proper prism layer treatment to correctly solve the boundary layer flow. In the inflow boundary (red surface in Fig. 2), two different conditions were used depending on the inflow velocity. In bollard pull cases with velocity equal to zero, a stagnation inlet, which imposes the total pressure, was considered; for the other cases (i.e., the free-flow conditions), a fixed velocity was preferred. In the outflow boundaries, a prescribed pressure condition was imposed, setting the pressure equal to the undisturbed one. Furthermore, an extrapolated backflow treatment has been adopted for these boundaries. In case an inflow is computed on these surfaces, its direction is extrapolated from the interior velocities. This approach aims to prevent unphysical boundary disturbances in the outlet surfaces.

A turbulent wall treatment was adopted according to the flow regime in the experimental campaign ($R_E > 4.4 \times 10^5$). The validity of this assumption was also confirmed because during experimental tests, roughness strips had been applied on the rudder nose to stimulate a turbulent flow (Molland and Turnock 1993b). As expected, the *Realizable k-ε* turbulent numerical model was used to close the RANS equations; moreover, the two-layer wall treatment with a $y+$ up to 60 (which was within the model confidence) was adopted.

For the mesh arrangements, a polyhedral mesh was generated with the Star-CCM+ mesher. This tool had the capability to include mesh refinements to increase the space accuracy in the region where higher flow gradients were expected (as near the rudder and in the zone influenced by the propeller effect). The reference mesh setup used in most of the following analyses consists of approximately one million cells. For each analyzed case (rudder in open-water and bollard pull conditions), a preliminary mesh sensitivity analysis was performed. This analysis was conducted considering the main aim of this study, that is, to propose an approach that may be applied in the preliminary design phases.

5 Results

As a preliminary (and fundamental) step, the reliability of the proposed tools to predict the performances of the propeller and the rudder separately (without interaction) was assessed. Based on this objective, the capability of the body-force approach to correctly simulate the propeller inflow field to the rudder was analyzed. Then, the rudder alone in a prescribed uniform flow velocity was considered to define the limits of application of the viscous code using a mesh that was not extremely computationally demanding. After these preliminary tests, the coupled rudder/propeller system in the propeller bollard pull condition was considered.

5.1 Open-Water Propeller

In the literature (Wang et al. 2008; Gaggero et al. 2010, 2014b; Shen and Su 2009; Gaggero and Villa 2016), extensive analyses of the reliability of viscous codes have been conducted to predict the propeller performance in a wide range around the design condition, and in some cases in proximity to the bollard pull condition. The findings show good agreement with the experimental results. The viscous solver was assumed to be a reliable tool and was used as a reference case to validate the body-force approach. Initially, the performance of the modified version of the Wageningen B-Series propeller (Molland and Turnock 1990) adopted in the experimental campaign was computed using the viscous solver; the results showed a very satisfactory overall accuracy, with discrepancies of approximately 1% in the experimental data for the thrust force (see Bruzzone et al. 2014). The load distribution along the blade computed in the full RANS calculations was then used to generate a radially varying actuator disk. Owing to software constraints, a polynomial function was used to feed the body-force field to the viscous code. In particular, two 11th-order polynomial curves were used to correctly fit the reported data. The computed load and polynomial fitting distributions are reported in Fig. 3. As expected, due to the high loading condition (bollard pull), the blade load distribution shifted toward higher radii in the usual design condition. On the contrary, the tangential load component presented a more uniform distribution.

The comparison of the circumferential average velocity components (in axial and tangential directions) evaluated considering the fully resolved propeller and the simplified model is reported in Figs. 4 and 5. These two flow components are the main ones that affect the local rudder inflow angle. The simulations in the two cases were conducted by adopting the same mesh arrangement to preserve the same space accuracy in the propeller wake region. The propeller zone, where a finer body-fitted mesh has been used in the full RANS calculations to include the real blade geometry, is the only
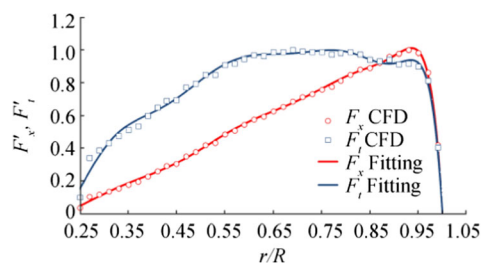

Fig. 3 Used nondimensional load distribution (solid lines) compared with computed nondimensional distribution with full RANS simulation (dots) of longitudinal (red) and tangential (blue) forces
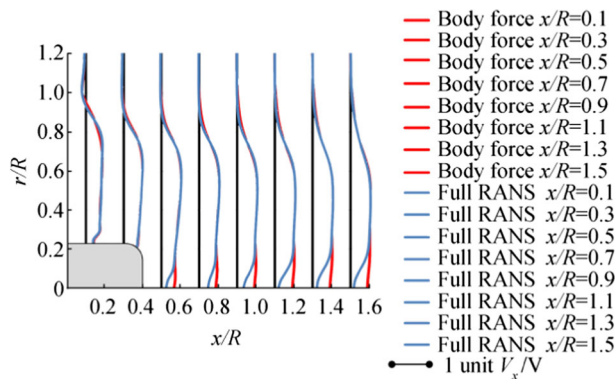
Fig. 4 Comparison of propeller wake velocity profile at different longitudinal sections (from 0.1R to 1.5R with a step of 0.2). Full RANS computation (blue) compared with body force (red) (axial component)

exception. The two approaches show good agreement for almost all of the considered longitudinal positions, demonstrating the accuracy of the proposed method. In particular, in Figs. 4 and 5, the position of the transversal planes and velocity field (axial or tangential) are reported on the x-axis, while the nondimensional radial coordinate is reported on the y-axis. Given the axial component (Fig. 4), certain discrepancies are visible in the inner radii, where the presence of the hub vortex (obviously not reproduced in the body-force model) generates a significant velocity reduction.

Similarly, in the outer radii (r/R close to 1), the unresolved tip vortex results in small discrepancies between the two simulations; these are evident in the section nearest to the propeller ($x/R = 0.1$). With the tangential component (Fig. 5), the same differences are again visible at the inner and outer radii, but in this case, they are more marked at the outer radii for the section nearest to the propeller. Notwithstanding these differences, a good agreement has been observed for both components, which represent the main contribution to the rudder inflow field. The mean downstream velocities show that the
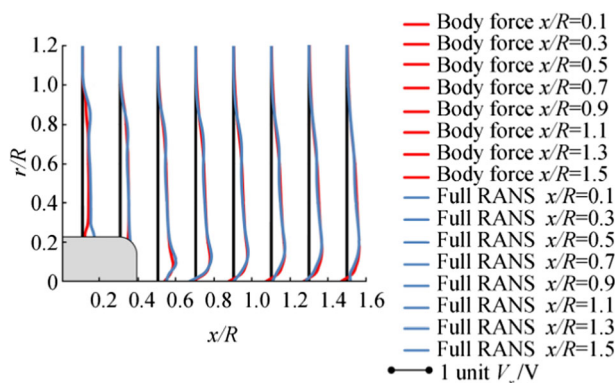
wake contraction is well predicted, making the body-force approach a fast and reliable method to generate an accurate inflow field to the rudder in this complex condition. The same conclusions may be obtained from Fig. 6, where the axial wakes are reported for three longitudinal positions (namely, 0.3, 0.5, and 1.1R downstream). In the full RANS simulation, the periodic nature of the wake generated by the four-bladed propeller is evident. On the contrary, the radially varying body force produces a circumferentially uniform flow, as expected. This result obviously eliminates the flow unsteadiness to the rudder (and consequently the force fluctuations), but no detrimental effect on the mean component is present, as shown in the next section. The steady calculations allowed by the inclusion of the body force into the simulation via the radially varying actuator disk (in place of the unsteady approach needed in case of the fully resolved RANS propeller) can drastically reduce the computational time, which may decrease by up two orders of magnitude.
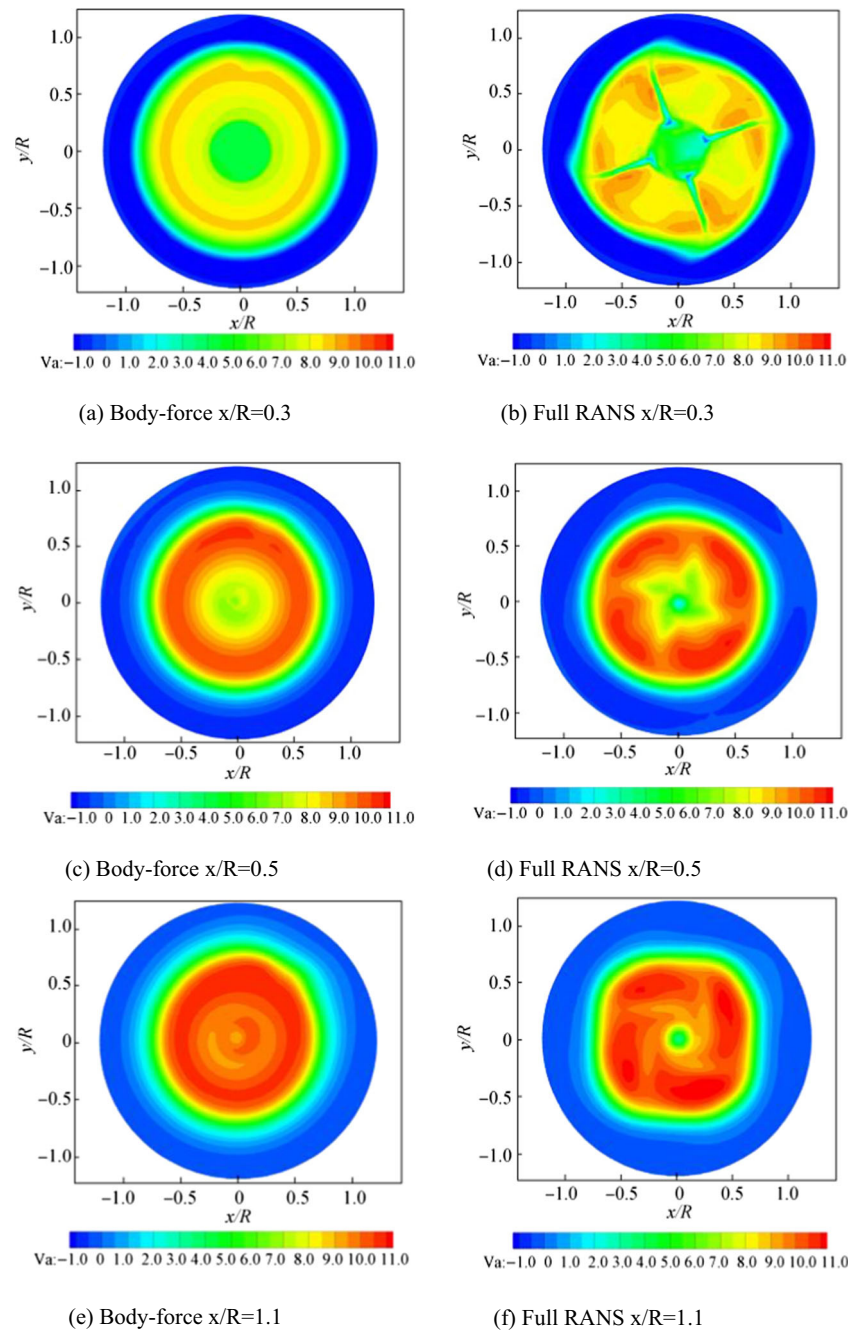
Despite the evident advantages of the proposed method, its main problem to be effectively used in front of a rudder is related to the necessity of feeding the model with a reliable blade load distribution. This issue was demonstrated by Bruzzone et al. (2014), who analyzed a simpler setup with the propeller at a lower loading condition. In particular, mean flow fields that correspond to different propeller load distributions were considered, showing significant differences. In principle, many methods can be used to estimate the propeller load, ranging from simple potential code or BEMT methods to viscous computations. In the present case, the load distributions computed by means of RANS code are used to reproduce, as much as possible, the real one. At the early design stages, when the blade geometry might be unavailable, the radial load distribution could be estimated considering stock or literature propellers choosing the most appropriate case. If the choice is correctly made by adopting a propeller sufficiently similar to the final one, this approach can be considered reliable without an extremely large effect on the global rudder forces.

5.2 Open-Water Rudder

In the previous section, the capability of the simplified propeller model to generate a sufficiently accurate inflow field to the rudder was demonstrated. This section focuses on the open-water rudder performances. Based on the work of Molland and Turnock (1993a), two values of the inflow speed are considered, namely, 10 and 20 m/s, corresponding to a Reynolds number of 4.4×10^5 and 8.8×10^5, respectively.

As a preliminary step, a mesh sensitivity analysis has been conducted for two values of the flow angle of attack to the rudder (namely, 15° and 30°), representing two characteristic conditions, i.e., pre-stall and post-stall. These conditions present completely different flow characteristics: in the first, a smooth flow around the rudder is present; after the stall, a


Fig. 5 Comparison of propeller wake velocity profile at different longitudinal sections (from 0.1R to 1.5R with a step of 0.2). Full RANS computation (blue) compared with body force (red) (tangential component)

Fig. 6 Axial wake sections on (left) body-force model and (right) full RANS simulation

(a) Body-force x/R=0.3

(b) Full RANS x/R=0.3

(c) Body-force x/R=0.5

(d) Full RANS x/R=0.5

(e) Body-force x/R=1.1

(f) Full RANS x/R=1.1

large region with separated flow is present. For each condition, four additional meshes are generated, starting from the reference one. Two have been created systematically halving the cell count and two doubling it. With the adopted unstructured mesh, this result has been obtained by setting a smaller and a larger cell reference size. Note that further mesh refinements were not considered because doing so would have raised the computational costs beyond the scope of this study.

The results in terms of lift and drag forces in the adopted mesh setup are shown in Figs. 7 and 8. In particular, the computed values are reported in nondimensional form using the correspondent experimental value as reference. As regards the pre-stall condition (rudder angle of attack equal to 15°, indicated by red bars in the figures), even if the mesh size varies from approximately 300 000 to 3 million cells, the lift is always well predicted, with a discrepancy such that the experimental measurement is lower than 3% for the coarser mesh. Furthermore, the drag force is satisfactorily predicted even if in this case, a slightly larger variation is visible when moving from the coarsest to the finest mesh; best results are obtained with the fine and very fine mesh configurations. With the coarsest mesh, the error increases up to 7% (larger than that
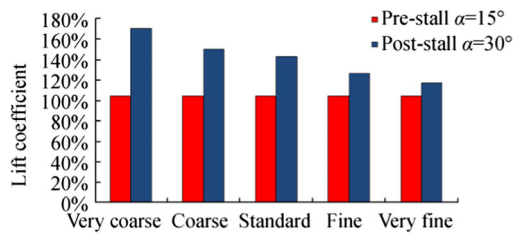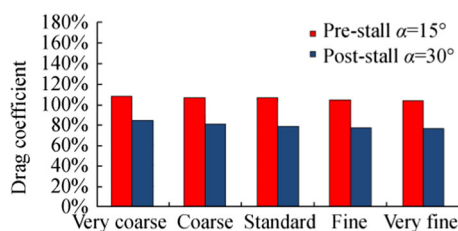
Fig. 7 Mesh sensitivity analysis for lift coefficient: red bars indicate pre-stall (15°) and blue bars show post-stall (30°) conditions

observed for the lift) but in accordance with similar numerical calculations even in finer meshes as shown by Badoe et al. (2015). The finest mesh requires approximately 10 times higher computational effort with respect to the coarsest one (as the computational time is nearly proportional to the cell count) but increases the accuracy to 4% for the drag and only 0.5% for the lift. As the lift force is definitely the most important component, the reference mesh can be considered adequate in terms of efficiency (accuracy over computational costs) in this rudder angle.

For the post-stall region (30°), various results were obtained. The current model is unable to correctly evaluate the force values (for both lift and drag). Moreover, in the pre-stall region, results are strongly dependent on the mesh arrangement. This condition may be attributed to the complex flow developing around the rudder, with a large recirculating region. A closer look at the results shows that the lift (generally overestimated) varies from nearly 170% (coarsest mesh) to slightly less than 120% of the experimental value (finest mesh). The trend with increasing mesh size appears to progressively shift toward the experimental value, even if no proper convergence is achieved by using the finest mesh. For the drag (generally underestimated), a divergent trend is shown despite lower force variations with the mesh.

The discrepancies can be attributed to various numerical/flow problems. When large boundary layer separation occurs (as in the present case), strong flow unsteadiness is present. Thus, using a steady solver is inadequate for this type of simulations. However, in a previous work (Bruzzone et al. 2014), unsteady simulations were performed with the same mesh size (the
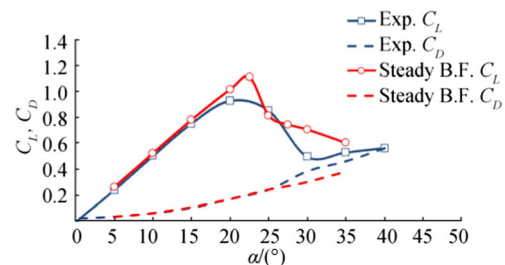
reference one), showing no significant improvements for this flow regime; this result allows us to hypothesize that, to correctly consider the flow unsteadiness, a finer mesh would be needed. A second possible reason for this discrepancy could be related to the near-wall flow. When strong boundary separations occur, the prediction of the separation point is important; it is numerically influenced both by the near-wall flow solution and the turbulence phenomena. Both aspects remain a challenge for CFD codes, particularly when smooth surfaces are involved in a stall region. Therefore, further investigation is needed where the separation point is unknown. Also in this case, a refined mesh would contribute to improving the quality of the result.

Although the adoption of a finer mesh could have been beneficial in the post-stall angle, the reference mesh is retained for the successive calculations. Indeed, in the preliminary design phases, correctly capturing the rudder behavior is important in pre-stalling conditions, while it may be considered acceptable to have discrepancies in the stalling region as long as the stall phenomenon is evidenced.

After this preliminary mesh sensitivity analysis, systematic calculations were conducted for the two velocities considered in the experimental campaign (10 and 20 m/s), which adopted the reference mesh.

The numerical and experimental results are reported in Figs. 9 and 10. In both figures, all available experimental data are reported (up to 40° and 50°, respectively, for the flow speeds of 10 and 20 m/s, with a step of 5° apart in the correspondence of very small angles of attack). Numerical calculations were limited to an angle of attack equal to 35°, with a step of 5° to avoid stressing the tool for higher angles of attack, where its accuracy is lower (as shown subsequently). A finer step (2.5°) was considered for numerical calculations to effectively characterize the stall region. In general, for both velocities, lift and drag forces are satisfactorily captured in the pre-stall conditions. In the post-stall angles, lift is significantly overpredicted while drag is underpredicted. This result confirms the inability of the present model with the adopted mesh size and arrangement to effectively simulate this particular

Fig. 8 Mesh sensitivity analysis for drag coefficient: red bars indicate pre-stall (15°) and blue bars show post-stall (30°) conditions

Fig. 9 Comparison of experimental (blue) and numerical (red) rudder forces for velocity of 10 m/s
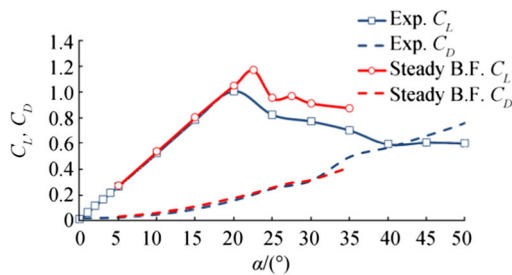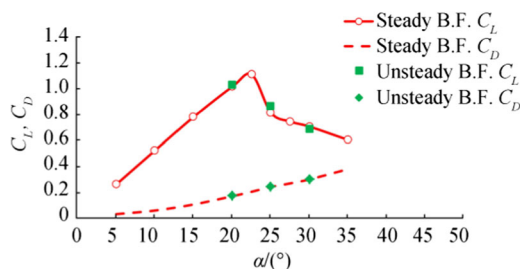
Fig. 10 Comparison of experimental (blue) and numerical (red) rudder forces for a velocity of 20 m/s

condition. Considering the stall inception (the angle of attack in which the stall occurs), the numerical code predicts an angle of 22.5° for both velocities. This value is near the experimental result (20°); moreover, that in the experimental data are present only for 20° and 25°, thereby precluding a precise evaluation of the experimental stall angle.

A further attempt has been conducted to improve the results of the post-stall condition. As stated, one of the main causes of the inaccuracy of the results in this region may be the neglected flow unsteadiness in the steady calculations. Thus, the more computationally demanding unsteady computations was conducted on three values of the rudder angle of attack in proximity to the stall zone (20°, 25°, and 30°). The results of these additional calculations are reported in Fig. 11. Even if the computational time was increased by more than 10 times (due to the adoption of a time step to fulfill the Courant number constraint), no significant improvements on the predicted forces were obtained by adopting the same mesh, thereby confirming the results reported by Bruzzone et al. (2014). In conclusion, neither the increase of the mesh size nor the inclusion of a time-accurate simulation led to a satisfactory prediction of the rudder performances in the post-stall region.

A potential source of error is the turbulence on the rudder surface. The stall inception is closely related to the amount of turbulence on the boundary layer, which can vary the detachment of the flow from the wall. Even if a deeper analysis of this aspect is desirable, further experimental measurements are needed to deeply understand this phenomenon and correctly calibrate numerical codes.
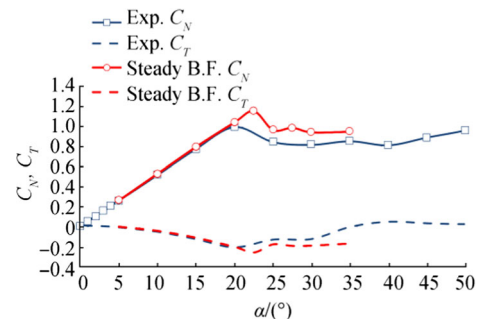
Furthermore, analyzing the results in terms of normal and tangential components with respect to the rudder plane (Figs. 12 and 13) is also useful. The same conclusions of the previous analyses can be drawn. In the pre-stall condition, both the components are in good agreement as long as the stall occurs. In the post-stall regime, the normal force shows a strong overprediction and the tangential one is underpredicted. This further confirms that when the strong recirculation occurs, the present model is inadequate to reliably compute the rudder forces differently from the pre-stall conditions. However, as stated, the post-stall region is less interesting from the point of view of ship maneuverability; thus, the proposed setup has been considered acceptable.

5.3 Propeller/Rudder Configuration

Once the capability of the code to analyze the two separated problems (rudder or propeller alone) had been assessed, the functioning behind the propeller of the rudder was considered to validate the procedure with regard to complex bollard pull conditions and assess its limits. In the considered configuration of the model tests, the propeller was located at a longitudinal distance from the rudder shaft equal to $0.39D$ without lateral displacement. The tests were performed with a propeller revolution rate of 755.5 r/min, considering a wide range of rudder angles, which vary in this case from 0° to 70° with a step of 5°. The previously presented blade load distribution was imposed in the radially varying actuator disk, forcing the global thrust and torque to be equal to the experimental data.

As previously performed for the open-water rudder, a mesh sensitivity analysis was also conducted for the coupled problem. For the reference mesh (approximately 1.02 million cells), a coarse one halved the cell count (approximately 562 000 cells) and two finer meshes doubled the total cell amount (approximately 2.32 and 3.72 million cells). Even if the previously reported results for the rudder alone showed the inadequacy of the mesh to compute the stall condition, in this particular operational condition, post-stall angles were considered, covering the entire experimental rudder range. However, in this case, a

Fig. 11 Comparison of steady (red) and unsteady (green) calculations for lower flow speed (10 m/s)

Fig. 12 Comparison of experimental (blue) and numerical (red) rudder forces for a velocity of 10 m/s, normal and tangential components
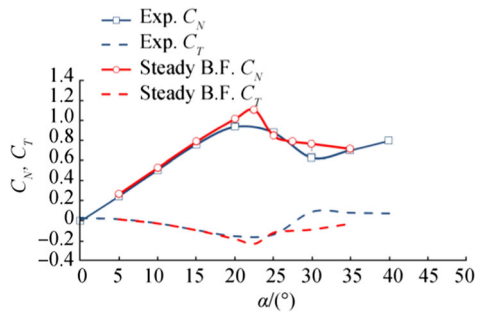
Fig. 13 Comparison of experimental (blue) and numerical (red) rudder forces for a velocity of 20 m/s, normal and tangential components

lower number of values of the rudder angle of attack was considered to limit the computational time. Specifically, a 10° step was adopted, adding a step to the computational calculation of 45° to effectively capture the behavior in the stall region.

Contrary to the rudder-alone case, where a strong dependence on the mesh was highlighted for the post-stall region, a much lower dependence was found for the coupled case. This result is evident in Fig. 14, which shows similar results even if a wide variation of cell numbers (between 0.5 and 4 million cells) has been explored. This result can be attributed to reasons such as the tangential flow components provided by the propeller or the presence of an accelerating device (such as the propeller) close to the rudder. Further studies on this aspect will be conducted in the future.

Once the mesh dependence was analyzed, a comparison between experimental measurements and numerical results was conducted, as reported in Fig. 15.

The results show a good agreement for the lift in the entire analyzed range. A slight overestimation occurs in the range between 20° and 40°, with differences of up to 10%–15%. In this range, the measured force loses its linear behavior with respect to the angle of attack; this condition can be attributed to minor recirculation effects on the rudder blade.

As shown in the previous simpler case, the present technique reasonably predicts the occurrence of the stall. In
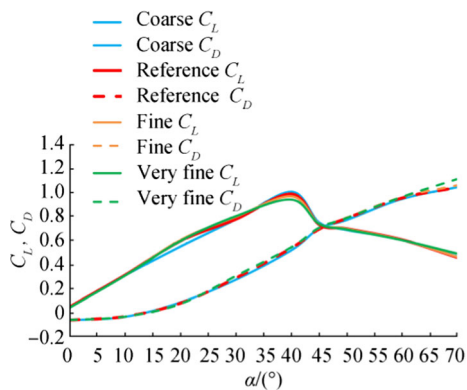
particular, the postponement of the stall inception with respect to the rudder-alone configuration is correctly captured. However, the stall is slight anticipated (40° instead of 45°).

With respect to the previous results, the post-stall region is effectively predicted up to the maximum analyzed angle both in terms of value (which is slightly overpredicted) and trend.

The drag component, differently, shows a larger discrepancy in the entire range. For the lower angles of attack (up to 15°), a negative drag force has been computed. Badoe et al. (2015) showed that this result was due to the swirl effect of the propeller in front of the rudder, which generates a negative induced drag (positive force). This beneficial effect was also observed in other experimental data provided by Molland and Turnock (1993a). From a theoretical point of view, this effect should be always present; it can be reduced (or completely overruled) by the viscous component of the drag, which acts in the opposite direction. In the present results, this phenomenon seems overpredicted, with a change in the sign of the force at the lowest angles of attack. Unfortunately, experimental tests cannot separate the forces in pressure and viscous component; thus, difficulty is encountered in defining whether the problem is due to an underestimation of the shear stress or an overprediction of the propeller swirl effect, even if one may hypothesize that the first is more important considering previous results.

The drag curve seems shifted for every angle, even if slightly compensated by the overprediction of the lift for the range between 20° and 40°. Given that the drag is strongly underestimated in the post-stall zone, based on the previous results for the free stream rudder and the good results for the lift, the findings may suggest that the proposed mesh setup is inadequate to predict the stress component of the force but is capable of adequately computing the pressure component. This conclusion may be supported by the results of the global mesh sensitivity. Mesh refinements mainly affect the pressure field or flow field out of the boundary layer. The low dependence of results on the mesh refinement suggests that an improved representation of the stress component should be achieved. Further analysis related to this problem is necessary.

Fig. 14 Mesh sensitivity analysis for rudder–propeller system (body-force approach)
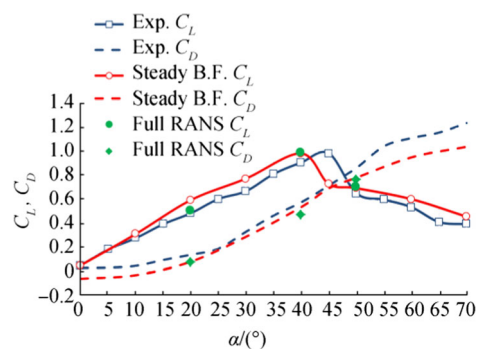
Fig. 15 Comparison between steady body-force approach numerical results (red), unsteady full RANS approach numerical results (green), and experimental measurements (blue): lift and drag forces

Thus, focused experiments to effectively analyze the accuracy of the boundary layer prediction should be conducted.

As proposed in the previous paragraph, the same results are also shown in terms of normal and tangential components in the rudder plane (Fig. 16). In this case, similar conclusions can be drawn. The computed normal component is in good agreement with the measured one, with only a small overprediction for the pre-stall region and a small underprediction in the post-stall regime. By contrast, for the entire analyzed range, the tangential force shows larger discrepancies, which confirm the previously reported conclusions. Nevertheless, considering that the normal force is dominant to the tangential one, the proposed model is able to fairly predict the effect of the propeller-accelerated flow on the developed rudder forces.

Another potential source of discrepancy between the measured and computed values is the adoption of the simplified approach to include the propeller. To verify this aspect also for this particular working condition, some specific full RANS simulations were conducted. The mesh setup used was based on the reference one with the inclusion of a body-fitted propeller mesh region. Unsteady computations were performed using the sliding mesh technique to consider the propeller revolution rate. These simulations required over 10 times more computational time on the same hardware with respect to the steady ones with the simplified propeller. In Fig. 15, the results obtained from the three analyzed values of the angles of attack (20°, 40°, and 50°) are reported (as indicated by green dots). For the lift force, a good agreement with the simplified model is found, with minor difference in the 20° where the full RANS simulation predicts a more accurate value. This discrepancy could be due to the effect of the unsteady flow to the rudder (neglected in the simplified model), which can stimulate the aforementioned recirculation phenomena. This condition also justifies the loss of the linear behavior of the force relative to the angle of attack recorded in the experimental data. This effect is higher in the small angles because the simplified model predicts large recirculating regions. For the drag force, the full RANS calculations exhibit similar

values and flow characteristics of the simplified model. This result confirms the previously reported considerations.

6 Conclusions

In the present study, the capability of a modern CFD tool (a RANS solver) to evaluate the interaction between the rudder and the propeller in bollard pull condition was explored. To ensure complete understanding, a preliminary analysis of the separate problems in the rudder and propeller was performed. For all the tested conditions, a mesh sensitivity analysis was conducted. Moreover, a comparison with the more demanding full RANS simulations and experimental data available in the literature was conducted.

The results related to the open-water rudder demonstrated a sufficient accuracy for a wide range of values of the angle of attack even if nonnegligible discrepancies exist particularly in the post-stall region. The adoption of a finer mesh or unsteady calculations did not allow a significant improvement of the results. The poor solution quality in the post-stall condition may be attributed mainly to an incorrect prediction of the flow separation point, which strongly influences the expected force.

To limit the computational cost, the propeller effect was introduced in a simplified manner through the body-force method. The initial validation of the propeller flow by means of the comparison with a full RANS simulation showed a good agreement in inflow to the rudder generated by the propeller. Even if the proposed simplification completely eliminates the blade unsteadiness, it can reduce the computational time by up to one order of magnitude in a full RANS unsteady simulation without significant detriment to the expected accuracy.

The coupled system exhibited fairly good results. The reported numerical results still present some nonnegligible discrepancies with respect to the experimental measurements. These discrepancies are likely unrelated to the simplification adopted and further investigation is necessary, possibly considering results from ad hoc experiments.

As a general conclusion, the proposed simplified approach was also sufficiently reliable in the complex bollard bull condition. This result allows the systematic use of this approach in other rudder types and/or geometries, with the aim of accurately generating a sufficiently large set of data in which new formulations can include the rudder–propeller interaction into the maneuvering model.
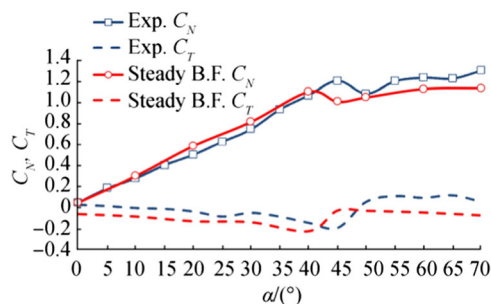
Fig. 16 Comparison of numerical (red) and experimental (blue) data: normal and tangential forces (steady body-force approach)

References

Abkowitz MA (1980) Measurement of hydrodynamic characteristics from ship maneuvering trials by system identifications. Society of

Naval Architects and Marine Engineers SNAME Trans. 88 (1), Jersey City, NJ United States 283–318

Badoe CE, Phillips AB, Turnock SR (2015) Influence of drift angle on the computation of hull-propeller-rudder interaction. Ocean Eng 103(2015):64–77. https://doi.org/10.1016/j.oceaneng.2015.04.059

Berger S, Druckenbrod M, Greve M, Abdel-Maksoud M, Greitsch L (2011) An efficient method for the investigation of propeller hull interaction. Proc.14th Numerical Towing Tank Symposium, Poole, United Kingdom

Bertram V (2002) Practical Ship Hydrodynamics. Buttherworth Heinemann. ISBN 0 7506 4851 1

Broglia R, Dubbioso G, Durante D, Di Mascio A (2013) Simulation of turning circle by CFD: analysis of different propeller models and their effect on manoeuvring prediction. Appl Ocean Res 39:1–10. https://doi.org/10.1016/j.apor.2012.09.001

Bruzzone D, Gaggero S, Podenzana Bonvino C, Villa D, Viviani M (2014) Rudder-propeller interaction: analysis of different approximation techniques. In Proceedings of the 11th international conference on hydrodynamics ICHD 2014, Singapore, October 19–24 2014, pp. 230–239, ISBN: 978-981-09-2175-0

Carlton J (2012) Marine propellers and propulsion. Butterworth-Heinemann. Print Book ISBN :9780080971230

Carlton J, Radosavljevic D, Whitworth S (2009) Rudder–propeller–hull interaction: the results of some recent research, In-Service Problems and Their Solutions First International Symposium on Marine Propulsors smp'09, Trondheim, Norway

CD-Adapco (n.d.) Star-CCM v.9 User manual. http://www.cd-adapco.com

Coraddu A, Dubbioso G, Mauro S, Viviani M (2013) Analysis of twin screw ships' asymmetric propeller behaviour by means of free running model tests. Ocean Eng 68:47–64, ISSN:0029-8018, Elsevier. https://doi.org/10.1016/j.oceaneng.2013.04.013

Crane LC, Eda H, Landsburg A (1989) Controllability. In: Principles of naval architecture. vol. 3. Editor: Edward V. Lewis, Published by The Society of Naval Architects and Marine Engineers Jersey City, NJ ISBN No. 0-939773-02-3

Di Mascio A, Dubbioso G, Muscari R, Felli F (2015) CFD analysis of propeller-rudder interaction. Proceedings of the Twenty-fifth International Ocean and Polar Engineering Conference Kona, Big Island, Hawaii, USA, June 21-26, 2015

Dubbioso G, Viviani M (2012) Aspects of twin screw ships semi-empirical maneuvering models. Ocean Eng 48:69–80, ISSN 0029-8018, Elsevier. https://doi.org/10.1016/j.oceaneng.2012.03.007

Dubbioso G, Mauro S, Ortolani F, Martelli M, Nataletti M, Villa D, Viviani M (2015) Experimental and numerical investigation of asymmetrical behaviour of rudder/propeller for twin screw Ships. In International Conference on Marine Simulation and Ship Maneuverability-MARSIM'15, September 8–11, Newcastle United kingdom

Durante D, Dubbioso G, Broglia R, Di Mascio A (2012) The turning-circle maneuver of a twin-screw vessel with different stern appendages configuration. 15th Numerical Towing Tank Symposium 7–9 October 2012 Cortona, Italy

Felli M, Roberto C, Guj G (2009) Experimental analysis of the flow field around a propeller-rudder configuration. Exp Fluids 46(1):147–164. https://doi.org/10.1007/s00348-008-0550-0

Fujii H, Tuda T (1961) Experimental researches on rudder performance. J Soc Naval Architects Jpn 109:105–111. https://doi.org/10.2534/jjasnaoe1952.1960.107_105

Gaggero S, Villa D (2016) Steady cavitating propeller performance by using OpenFOAM, StarCCM+ and a boundary element method. Proc IMechE Part M J Eng Mar Environ 231(2):411–440. https://doi.org/10.1177/1475090216644280

Gaggero S, Villa D, Brizzolara S (2010) RANS and PANEL method for unsteady flow propeller analysis. J Hydrodyn 22(5 SUPPL.1):547–552. https://doi.org/10.1016/S1001-6058(09)60253-5

Gaggero S, Villa D, Viviani M, Rizzuto E (2014a) Ship wake scaling and effect on propeller performances. Developments in maritime transportation and exploitation of sea resources—Proceedings of IMAM 2013, 15th International Congress of the International Maritime Association of the Mediterranean Volume 1, 2014, Pages 13–21 15th International Congress of the International Maritime Association of the Mediterranean, IMAM 2013; A Coruna; Spain; 14–17 October 2013 ISBN: 978-113800161-9

Gaggero S, Villa D, Viviani M (2014b) An investigation on the discrepancies between RANSE and BEM approaches for the prediction of marine propeller unsteady performances in strongly non-homogeneous wakes. Proceedings of the International Conference on Offshore Mechanics and Arctic Engineering – OMAE Volume 2, 2014 ASME 2014 33rd International Conference on Ocean, Offshore and Arctic Engineering, OMAE 2014; San Francisco; United States; 8 June 2014 through 13 June 2014; Code 109000. https://doi.org/10.1115/OMAE2014-23831

Gaggero S, Villa D, Viviani M (2015) The Kriso container ship (KCS) test case: an open source overview. MARINE 2015 - Computational Methods in Marine Engineering VI 2015, Pages 735–749 6th International Conference on Computational Methods in Marine Engineering, MARINE 2015; Consiglio Nazionale delle Ricerche (CNR)Rome; Italy; 15 June 2015 through 17 June 2015; ISBN: 978-849439286-3

Gaggero S, Villa D, Viviani M (2017) An extensive analysis of numerical ship self-propulsion prediction via a coupled BEM/RANS approach. Appl Ocean Res 66:55–78. https://doi.org/10.1016/j.apor.2017.05.005 ISSN: 01411187

Han K (2008) Numerical optimization of hull/propeller/rudder configurations. Doctor Thesis, Chalmers University of Technology, Gothenburg, Sweden. ISBN 978-91-7385-111-4

Hochbaum AC (1998) Computation of the turbulent flow around a ship model in steady turn and in steady oblique motion. In: Twenty-Second Symposium on Naval Hydrodynamics, August 9-14, Preprints, Washington DC. p 198–213

Katz J, Plotkin A (2001) Low-speed aerodynamics, vol 13. Cambridge University Press, Cambridge ISBN: 9780521665520

Kim WJ, Van SH, Kim DH (2001) Measurement of flows around modern commercial ship models. Exp Fluids 31(5):567–578. https://doi.org/10.1007/s003480100332

Krasilnikov VI, Berg A, Øye IJ (2003) Numerical prediction of sheet cavitation on rudder and podded propellers using potential and viscous flow solutions. In Proc. of the 5th Int. Symposium on Cavitation-CAV, pp 1–4

Lee H, Kinnas SA, Gu H, Natarajan S (2003) Numerical modeling of rudder sheet cavitation including propeller/rudder interaction and the effects of a tunnel. In Fifth international symposium on cavitation (CAV2003), Osaka, Japan, Vol. 14

Liu J, Hekkenberg R (2016) Sixty years of research on ship rudders: effects of design choices on rudder performance. Ships Offshore Struct 12, 2017(4):495–512. https://doi.org/10.1080/17445302.2016.1178205

Molland AF, Turnock SR (1990) Wind tunnel tests results for a model ship propeller based on a modified Wageninghen B4.40. Ship Science Report No. 43 University of Southampton, Southampton United Kingdom, ISSN 0140-3818

Molland AF, Turnock SR (1992) Further wind tunnel tests on the influence of propeller loading on ship rudder performance. Ship Science Report No. 52 University of Southampton, Southampton United Kingdom, ISSN 0140-3818

Molland AF, Turnock SR (1993a) Wind tunnel tests on the influence of propeller loading on ship rudder performance: four quadrant operation, low and zero speed operation. Ship Science Report No. 64 University of Southampton, Southampton United Kingdom, ISSN 0140-3818

Molland AF, Turnock SR (1993b) Wind tunnel investigation of the influence of loading on a semi-balanced skeg. Ship Science Report No.

48 University of Southampton, Southampton United Kingdom, ISSN 0140-3818

Molland AF, Turnock SR (2007) Marine rudders and control surfaces. 1st Edition p. 448 Butterworth-Heinemann, ISSN: 9780750669443

Norrbin NH (1971) Theory and observations on the use of a mathematical model for ship manoeuvring in deep and confined waters. Technical Report No. p. 123, SSPA-Pub-68. Swedish State Shipbuilding Experimental Tank Goteborg

Rijpkema D, Starke B, Bosschers J (2013) Numerical simulation of propeller-hull interaction and determination of the effective wake field using a hybrid RANS-BEM approach. In Third International Symposium on Marin Propulsors-SMP2013, Launceston, Tasmania, Australia, May 2013

Shen HL, Su YM (2009) Study of propeller unsteady performance prediction in ship viscous non-uniform wake. J Hydrodyn (Ser. A) 2: 017 ISSN: 1000-4874

Sheng H, Xiang-yuan Z, Chun-yu G, Xin C (2007) CFD simulation of propeller and rudder performance when using additional thrust fins. J Mar Sci Appln 6(4):27–31. https://doi.org/10.1007/s11804-007-7023-3

Simonsen C (2000) Propeller-rudder interaction by RANS. Ph.D. Thesis. Department of Naval Architecture and Offshore Engineering, University of Denmark, Denmark, Lyngby April 2000. ISBN: 87-89502-33-7

Simonsen CD, Stern F (2003) Verification and validation of RANS maneuvering simulation of Esso Osaka: effects of drift and rudder angle on forces and moments. Comput Fluids 32(10):1325–1356. https://doi.org/10.1016/S0045-7930(03)00002-1

Stern F, Kim HT, Zhang DH, Toda Y, Kerwin J, Jessup S (1994) Computation of viscous flow around propeller-body configurations: series 60 CB = 60 ship model. J Ship Res 38(2):137 ISSN: 00224502

Stern F, Agdrup K, Kim SY, Hochbaum AC, Rhee KP, Quadvlieg F, Perdon P, Hino T, Broglia R, Gorski J (2011) Experience from SIMMAN 2008-The first workshop on verification and validation of ship maneuvering simulation methods. J Ship Res 55(2):135–147 ISSN: 00224502

Villa D, Gaggero S, Brizzolara S (2011) Simulation of ship in self-propulsion with different CFD methods: From actuator disk to potential flow/RANS coupled solvers. RINA Royal Institution of Naval Architects -Developments in Marine CFD, London, pp 1–12

Wackers J, Deng G, Guilmineau E, Leroyer A, Queutey P, Visonneau M (2015) What is happening around the KVLCC2?. Proceedings of 18th Numerical Towing Tank Symposium 28–30 September 2015, Cortona, Italy

Wang C, Huang S, Xie XS (2008) Hydrodynamic performance prediction of some propeller based on CFD. J Nav Univ Eng 4:0–25